Comput. Mech. (2007) 39: 323–333
DOI 10.1007/s00466-006-0031-3

ORIGINAL PAPER

J. Sladek · V. Sladek · Ch. Hellmich
J. Eberhardsteiner

Heat conduction analysis of 3-D axisymmetric and anisotropic FGM bodies by meshless local Petrov–Galerkin method

Received: 28 April 2005 / Accepted: 29 November 2005 / Published online: 25 February 2006

Abstract The meshless local Petrov–Galerkin method is used to analyze transient heat conduction in 3-D axisymmetric solids with continuously inhomogeneous and anisotropic material properties. A 3-D axisymmetric body is created by rotation of a cross section around an axis of symmetry. Axial symmetry of geometry and boundary conditions reduces the original 3-D boundary value problem into a 2-D problem. The cross section is covered by small circular subdomains surrounding nodes randomly spread over the analyzed domain. A unit step function is chosen as test function, in order to derive local integral equations on the boundaries of the chosen subdomains, called local boundary integral equations. These integral formulations are either based on the Laplace transform technique or the time difference approach. The local integral equations are nonsingular and take a very simple form, despite of inhomogeneous and anisotropic material behavior across the analyzed structure. Spatial variation of the temperature and heat flux (or of their Laplace transforms) at discrete time instants are approximated on the local boundary and in the interior of the subdomain by means of the moving least-squares method. The Stehfest algorithm is applied for the numerical Laplace inversion, in order to retrieve the time-dependent solutions.

Keywords Transient heat conduction problem · Axisymmetric · Anisotropic functionally graded materials · Time-difference form, Laplace transform · Stehfest algorithm · Meshless approximation

J. Sladek (✉) · V. Sladek
Institute of Construction and Architecture,
Slovak Academy of Sciences,
84503 Bratislava, Slovakia
E-mail: sladek@savba.sk

Ch. Hellmich · J. Eberhardsteiner
Institute for Mechanics of Materials and Structures,
Vienna University of Technology,
Karlsplatz 13/202, 1040 Wien, Austria

1 Introduction

Functionally graded materials (FGMS) are multi-phase materials with the phase volume fractions varying gradually in space, in a pre-determined profile. This results in continuously graded thermomechanical properties at the (macroscopic) structural scale. Often, these spatial gradients in material behavior render FGMs as superior to conventional composites. FGMs posses some advantages over conventional composites because of their continuously graded structures and properties [19, 29]. FGMs may exhibit isotropic or anisotropic material properties, depending on the processing technique and the practical engineering requirements. Frequent use of FGMs for structures under thermal load motivates analysis of the temperature distribution in such materials. The optimum design of FGMs with respect to their thermal stress resistance requires the mathematical solutions for the thermomechanics of FGMs with arbitrarily graded material properties. Literature on heat conduction problems in FGM materials is mostly focused on problems with exponential variations of thermal properties, formulated in Cartesian coordinates under stationary boundary conditions [11, 13, 21]. Transient heat transfer in FGMs with the exponential spatial variation has also been examined [12, 14, 15, 22, 30].

Due to the high mathematical complexity of the initial-boundary value problems, analytical approaches for the thermomechanics of FGMs are restricted to simple geometry and boundary conditions. Thus, the transient heat conduction analysis in FGM demands accurate and efficient numerical methods. The finite element method can be successfully applied to problems with an arbitrary variation of material properties by using special graded elements [16]. In commercial computer codes, however, material properties are considered to be uniform on each element. The boundary element method (BEM) is a suitable numerical tool for this purpose too. However, to the knowledge of the authors, only Sutradhar et al. [30] applied the BEM to 3-D transient heat conduction analysis in FGM, where the Green's function approach and an exponential variation of material parameters were used. Up to date no special BEM has been presented in literature to

analyze 3-D axisymmetric functionally graded bodies. Only homogeneous problem was investigated by Brebbia et al. [5]. The conventional boundary integral formulation in the time-domain requires a complex fundamental solution proportional to the modified Bessel function of the first kind. A pure BEM formulation can be applied only to problems, where fundamental solutions are available. For a general nonhomogeneous body the fundamental solution for transient heat conduction problem is yet not known in literature. One possibility to obtain a BEM formulation is based on the use of fundamental solutions for a fictitious homogeneous medium, as has been suggested for the first time by Butterfield [6] for potential flow problems. This approach, which is the basis of the global BEM, however, leads to a boundary-domain integral formulation with additional domain integrals for the gradients of primary fields to obtain a unique formulation. This integral formulation valid for the global domain has been applied to the heat conduction analysis in nonhomogeneous media by Tanaka and Tanaka [31]. The price to be paid in such an approach is the loss of a pure boundary integral character of the formulation. Evaluation of integrals on the global domain brings some computational difficulties. Albeit the great success of the finite and boundary element methods as effective numerical tools for the solution of boundary value problems on complex domains, resting shortcomings of these methods still distill growing interest in development of new advanced computational methods.

In particular, meshless formulations are becoming popular, due to their high adaptivity and a low cost to prepare input data for numerical analyses. A significant number of such methods have been proposed so far [2–4]. The analyzed domain can be divided into small subdomains with a simple, e.g. circular, geometry. To each subdomain one can relate the fundamental solution of some simplified differential operators or of a parametrix (Levi function), instead of the fundamental solutions [10, 32]. On the surface of subdomains the local boundary integral equations (LBIEs) are written in the Laplace transform domain to eliminate the time dependence of the governing equation for transient heat conduction problems. This idea was applied to 2-D transient heat conduction analysis [18, 23, 26]. Authors applied that approach to analyze transient heat conduction problems in 3-D axisymmetric and isotropic functionally graded solids [24]. The anisotropy increases the number of heat conduction constants, which renders the derivation of fundamental solutions as difficult even in a homogeneous case. Sladek et al. [25] proposed the meshless method based on the local Petrov–Galerkin approach to solve stationary and transient heat conduction problems in 2-D for anisotropic FGM.

In this paper, the meshless local Petrov–Galerkin (MLPG) method is applied to transient heat conduction problems in 3-D axisymmetric solids with continuously nonhomogeneous and anisotropic material properties. A 3-D axisymmetric body is created by the rotation of the cross section around the axis of symmetry. Axial symmetry of the geometry and boundary conditions reduces the original 3-D boundary value problem to a 2-D problem. Therefore, it is sufficient to analyze only the cross section, which is covered by small circular subdomains surrounding nodes randomly spread over the analyzed domain. A unit step function is chosen as the test function to derive local integral equations on boundaries of the chosen subdomains. There are two ways of eliminating the time variable in the differential equation. The first of them consists of elimination of the time derivative by using Laplace transformations. In the second approach, the finite difference interpolation for the time variation of the temperature field is used, in order to convert the linear parabolic differential equation into a linear elliptic differential equation [8]. For 3-D axisymmetric problem the LBIEs have a boundary-domain integral form. In contrast to the global BEM based on boundary-domain integral formulation the present boundary-domain integral formulation for simple subdomains does not imply any difficulties. The local integral equations are nonsingular and take a very simple form. Spatial variation of the Laplace transforms or the time-discrete temperature and the heat flux on the subdomain are approximated by means of the moving least-squares (MLS) method. Several quasi-static boundary value problems are solved for various values of the Laplace transform parameter. The Stehfest [28] numerical inversion method is applied to obtain the time-dependent solutions. Numerical examples for functionally graded full and hollow cylinders with an exponential spatial variation of thermal conductivity and diffusivity are presented to verify the proposed numerical method.

2 Local boundary integral equations

Consider a boundary value problem for the heat conduction problem in a continuously nonhomogeneous anisotropic medium, which is described by the governing equation:

$$\rho(\mathbf{x})c(\mathbf{x})\frac{\partial\theta}{\partial t}(\mathbf{x},t)=\left[k_{ij}(\mathbf{x})\theta_{,j}(\mathbf{x},t)\right]_{,i}+Q(\mathbf{x},t), \tag{1}$$

where $\theta(\mathbf{x},t)$ is the temperature field, $Q(\mathbf{x},t)$ is the density of body heat sources, k_{ij} is the thermal conductivity tensor, $\rho(\mathbf{x})$ is the mass density, and $c(\mathbf{x})$ is the specific heat.

For an axisymmetric problem, it is convenient to use cylindrical coordinates $\mathbf{x}\equiv(r,\varphi,z)$(Fig. 2). In this case, the governing equation (1) can be rewritten in the form

$$\left[k_{ij}(\mathbf{x})\theta_{,j}(\mathbf{x},t)\right]_{,i}+\frac{k_{rz}(\mathbf{x})}{r}\theta_{,z}(\mathbf{x},t)+\frac{k_{rr}(\mathbf{x})}{r}\theta_{,r}(\mathbf{x},t)+Q(\mathbf{x},t)=\rho(\mathbf{x})c(\mathbf{x})\frac{\partial\theta}{\partial t}(\mathbf{x},t), \tag{2}$$

where the summation convention for repeated indices i, j, representing the coordinates r, z, is assumed. Two different approaches will be applied to solve the governing equation (2).

The following boundary and initial conditions are assumed

$$\theta(\mathbf{x},t)=\tilde{\theta}(\mathbf{x},t),\quad \text{on}\quad \Gamma_{\theta},$$
$$q(\mathbf{x},t)=k_{ij}(\mathbf{x})\theta_{,j}(\mathbf{x},t)n_i(\mathbf{x})=\tilde{q}(\mathbf{x},t),\quad \text{on}\quad \Gamma_{q},$$
$$\theta(\mathbf{x},t)|_{t=0}=\theta(\mathbf{x},0)\ \text{and}\ \dot{\theta}(\mathbf{x},t)\big|_{t=0}=\dot{\theta}(\mathbf{x},0)\quad \text{in}\ \Omega,$$

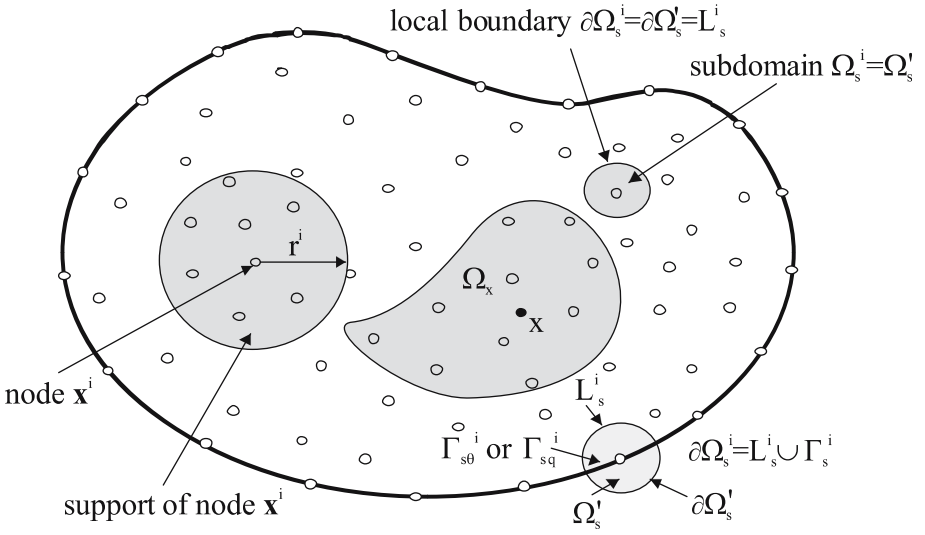

Fig. 1 Local boundaries for weak formulation (5) or (10), the domain Ω_x for moving least squares (MLS) approximation (11) of the trial function $\theta(\mathbf{x})$, and support area of weight function (18) around node $\mathbf{x}^i$

where Γ_θ is the part of the global boundary with prescribed temperature (see Fig. 1), while on Γ_q the heat flux is given, and n_i are the components of the unit outward normal vector to the boundary.

2.1 Laplace transform formulation

Applying the Laplace transform

$$\mathcal{L}[\theta(\mathbf{x},t)] = \bar{\theta}(\mathbf{x},s) = \int_0^\infty \theta(\mathbf{x},t)\mathrm{e}^{-st}\mathrm{d}\tau,$$

to Eq. (2) we get

$$\left[k_{ij}(\mathbf{x})\bar{\theta}_{,j}(\mathbf{x},s)\right]_{,i} + \frac{k_{rz}(\mathbf{x})}{r}\bar{\theta}_{,z}(\mathbf{x},s) + \frac{k_{rr}(\mathbf{x})}{r}\bar{\theta}_{,r}(\mathbf{x},s) + \bar{F}(\mathbf{x},s) = \rho(\mathbf{x})c(\mathbf{x})\bar{\theta}(\mathbf{x},s), \tag{3}$$

where s is the Laplace transform parameter and

$$\bar{F}(r,z,s) = \bar{Q}(r,z,s) + \theta(r,z,0)$$

is the redefined body heat source in the Laplace transform domain with the initial boundary condition for the temperature field $\theta(r,z,0)$. In this analysis, quantities in the Laplace transform domain are denoted by an over-bar.

Instead of writing the global weak form for the above governing equation, the MLPG methods construct the weak form over local subdomains such as Ω_s, which is a small region taken for each node inside the global domain [3]. The local subdomains overlap each other, and cover the whole global domain Ω (Fig. 1). The local subdomains could be of any geometric shape and size. In the current paper, the local subdomains are taken to be of circular shape. The local weak form of the governing equation (3) for $\mathbf{x}^i \in \Omega_s^i$ can be written as

$$\int_{\Omega_c^i} \left[\left(k_{ij}(\mathbf{x})\bar{\theta}_{,j}(\mathbf{x},s)\right)_{,i} + \frac{k_{rz}(\mathbf{x})}{r}\bar{\theta}_{,z}(\mathbf{x},s) + \frac{k_{rr}(\mathbf{x})}{r}\bar{\theta}_{,r}(\mathbf{x},s) - \rho(\mathbf{x})c(\mathbf{x})s\,\bar{\theta}(\mathbf{x},s) + \bar{F}(\mathbf{x},s)\right]\theta^*(\mathbf{x})\,\mathrm{d}\Omega = 0, \tag{4}$$

where $\theta^*(\mathbf{x})$ is a weight (test) function.

Applying the Gauss divergence theorem to Eq. (4) one can write

$$\begin{aligned}&\int_{\partial\Omega_s^i} \bar{q}(\mathbf{x},s)\theta^*(\mathbf{x})\mathrm{d}\Gamma - \int_{\Omega_s^i} k_{ij}(\mathbf{x})\bar{\theta}_{,j}(\mathbf{x},s)\theta^*_{,i}(\mathbf{x})\mathrm{d}\Omega \\ &- \int_{\Omega_s^i} \rho(\mathbf{x})c(\mathbf{x})s\bar{\theta}(\mathbf{x},s)\theta^*(\mathbf{x})\mathrm{d}\Omega + \int_{\Omega_s^i}\left[\frac{k_{rz}(\mathbf{x})}{r}\bar{\theta}_{,z}(\mathbf{x},s) + \frac{k_{rr}(\mathbf{x})}{r}\bar{\theta}_{,r}(\mathbf{x},s)\right]\theta^*(\mathbf{x})\mathrm{d}\Omega + \int_{\Omega_s^i}\bar{F}(\mathbf{x},s)\theta^*(\mathbf{x})\mathrm{d}\Omega = 0,\end{aligned} \tag{5}$$

where $\partial\Omega_s^i$ is the boundary of the local subdomain and

$$\bar{q}(\mathbf{x},s) = k_{ij}(\mathbf{x})\bar{\theta}_{,j}(\mathbf{x},s)n_i(\mathbf{x})$$

is the Laplace transform of the heat flux. The local weak form (5) is a starting point to derive LBIEs if an appropriate test function is selected. Aunit step function can be used as the test function $\theta^*(\mathbf{x})$ in each subdomain

$$\theta^*(\mathbf{x}) = \begin{cases} 1 & \text{at} \quad \mathbf{x} \in (\Omega_s \cup \partial\Omega_s) \\ 0 & \text{at} \quad \mathbf{x} \notin \Omega_s. \end{cases} \tag{6}$$

Then, the local weak form (5) is transformed into a simple LBIE

$$\int_{\partial\Omega_s^i} \bar{q}(\mathbf{x},s)\mathrm{d}\Gamma - \int_{\Omega_s^i} \rho(\mathbf{x})c(\mathbf{x})s\bar{\theta}(\mathbf{x},s)\mathrm{d}\Omega + \int_{\Omega_s^i}\left[\frac{k_{rz}(\mathbf{x})}{r}\bar{\theta}_{,z}(\mathbf{x},s)+\frac{k_{rr}(\mathbf{x})}{r}\bar{\theta}_{,r}(\mathbf{x},s)\right]\mathrm{d}\Omega = -\int_{\Omega_s^i}\bar{F}(\mathbf{x},s)\mathrm{d}\Omega \tag{7}$$

In the MLPG method the test and trial function, $\theta^*(\mathbf{x})$ and $\bar{\theta}(\mathbf{x},s)$, are not necessarily from the same functional spaces. The test function is chosen as the unit step function with support on the local subdomain. The trial function, on the other hand, is chosen to be the MLS interpolation over anumber of nodes randomly spread within the domain of influence, as described in greater detail in Sect. 3. While the local subdomain is defined as the support of the test function on which the integration is carried out, the domain of influence is defined as a region where the weight function is not zero and all nodes lying inside are considered for interpolation.

2.2 Time difference formulation

In this approach, we use the linear interpolation for the time variation of the temperature field and the partial differential Eq. (2) is converted into the following system of equations:

$$\left[k_{ij}(\mathbf{x})\theta_{,j}^{(n)}(\mathbf{x})\right]_{,i}+\frac{k_{rz}(\mathbf{x})}{r}\theta_{,z}^{(n)}(\mathbf{x})+\frac{k_{rr}(\mathbf{x})}{r}\theta_{,r}^{(n)}(\mathbf{x})+Q(\mathbf{x},t) = \rho(\mathbf{x})c(\mathbf{x})\frac{1}{\Delta t}\left[\theta^{(n)}(\mathbf{x})-\theta^{(n-1)}(\mathbf{x})\right], \quad (n=1,2,\ldots,N), \tag{8}$$

where the backward difference scheme for the time derivative of the temperature is applied, and $\theta^{(n)}(\mathbf{x})$ denotes the value of the temperature at a point $\mathbf{x}$ and the time instant $t_n = n\Delta t$.

Following the procedure used in the previous paragraph one can derive the integral representation of temperature in the nth time step. The local weak form of the governing Eq. (8) for $\mathbf{x}^i \in \Omega_s^i$ can be written as

$$\int_{\Omega_s^i}\left[\left(k_{ij}(\mathbf{x})\theta_{,j}^{(n)}(\mathbf{x})\right)_{,i}+\frac{k_{rz}(\mathbf{x})}{r}\theta_{,z}^{(n)}(\mathbf{x})+\frac{k_{rr}(\mathbf{x})}{r}\theta_{,r}^{(n)}(\mathbf{x}) - \rho(\mathbf{x})c(\mathbf{x})\frac{1}{\Delta t}\theta^{(n)}(\mathbf{x})+\rho(\mathbf{x})c(\mathbf{x})\frac{1}{\Delta t}\theta^{(n-1)}(\mathbf{x}) + Q(\mathbf{x},t)\right]\theta^*(\mathbf{x})\,\mathrm{d}\Omega = 0. \tag{9}$$

Similarly to the Laplace transform formulation, the local weak form (9) is transformed into a simple local boundary integral equation

$$\int_{\partial\Omega_s^i} q^{(n)}(\mathbf{x})\mathrm{d}\Gamma - \frac{1}{\Delta t}\int_{\Omega_s^i}\rho(\mathbf{x})c(\mathbf{x})\left[\theta^{(n)}(\mathbf{x})-\theta^{(n-1)}(\mathbf{x})\right]\mathrm{d}\Omega + \int_{\Omega_s^i}\left[\frac{k_{rz}(\mathbf{x})}{r}\theta_{,z}^{(n)}(\mathbf{x})+\frac{k_{rr}(\mathbf{x})}{r}\theta_{,r}^{(n)}(\mathbf{x})\right]\mathrm{d}\Omega = -\int_{\Omega_s^i}Q(\mathbf{x},t)\mathrm{d}\Omega, \tag{10}$$

where $q^{(n)}(\mathbf{x}) = k_{ij}(\mathbf{x})\theta_{,j}^{(n)}(\mathbf{x})n_i(\mathbf{x})$.

For the first time step, i.e., $n = 1$, the value $\theta^{(0)}(\mathbf{x})$ is given by the initial condition for the temperature distribution. Applying a spatial approximation for the temperature, the local integral equation (10) is transformed into the system of algebraic equation with unknown quantities at nodes used for spatial approximation, as described in Sect. 3. The system of algebraic equations is solved by step by step technique with respect to the time stepping.

3 Numerical solution

In general, a meshless method uses a local interpolation to represent the trial function with the values (or the fictitious values) of the unknown variable at some randomly located nodes. The MLS approximation [4, 17, 20] used in the present analysis may be considered as one of such schemes. Let us consider a sub-domain Ω_x of the problem domain Ω, in the neighbourhood of a point $\mathbf{x}$, for definition of the MLS approximation of the trial function (i.e. the actual temperature distribution) around x (Fig. 1). To approximate the distribution of the Laplace transform of temperature in Ω_x over a number of randomly located nodes $\{\mathbf{x}^a\}, a = 1, 2, \ldots n$, the MLS approximant $\bar{\theta}^h(\mathbf{x},s)$ of $\bar{\theta}$, $\forall\mathbf{x}\in\Omega_x$, is defined by

$$\bar{\theta}^h(\mathbf{x},s) = \mathbf{p}^{\mathrm{T}}(\mathbf{x})\mathbf{a}(\mathbf{x},s),\ \forall\mathbf{x}\in\Omega_x, \tag{11}$$

where $\mathbf{p}^{\mathrm{T}}(\mathbf{x}) = \left[p^1(\mathbf{x}),\ p^2(\mathbf{x}),\ldots,p^m(\mathbf{x})\right]$ is a complete monomial basis of order m; and $\mathbf{a}(\mathbf{x})$ is a vector containing the coefficients $a^j(\mathbf{x})$, $j = 1, 2, \ldots, m$ which are functions of the space co-ordinates $\mathbf{x} = [x_1,\ x_2,\ x_3]^{\mathrm{T}}$. For example, for a 2-D problem

$$\mathbf{p}^{\mathrm{T}}(\mathbf{x}) = [1,\ x_1,\ x_2], \text{ for linear basis } m = 3 \tag{12a}$$

$$\mathbf{p}^{\mathrm{T}}(\mathbf{x}) = \left[1,\ x_1,\ x_2,\ (x_1)^2,\ x_1x_2,\ (x_2)^2\right], \text{ for quadratic basis } m = 6 \tag{12b}$$

Similarly to Eq. (11) one can write approximation of $\theta^{(n)}(\mathbf{x})$ in the time difference formulation. The coefficient vector $\mathbf{a}(\mathbf{x})$ is determined by minimizing a weighted discrete L_2-norm defined as

$$J(\mathbf{x}) = \sum_{a=1}^{n} w^a(\mathbf{x})\left[\mathbf{p}^{\mathrm{T}}(\mathbf{x}^a)\mathbf{a}(\mathbf{x},s)-\hat{\theta}^a(s)\right]^2, \tag{13}$$

where $w^a(\mathbf{x})$ is the weight function associated with the node a with $w^a(\mathbf{x}) > 0$. Recall that n is the number of nodes in Ω_x for which the weight function $w^a(\mathbf{x}) > 0$ and $\hat{\theta}^a(s)$ are the fictitious nodal values, but not the nodal values of the unknown trial function $\bar{\theta}^h(\mathbf{x}, s)$ in general. The stationarity of J in Eq. (13) with respect to $\mathbf{a}(\mathbf{x}, s)$

$$\partial J/\partial \mathbf{a} = 0$$

leads to the following linear relation between $\mathbf{a}(\mathbf{x}, s)$ and $\hat{\theta}(s)$

$$\mathbf{A}(\mathbf{x})\mathbf{a}(\mathbf{x}, s) - \mathbf{B}(\mathbf{x})\hat{\theta}(s) = 0, \tag{14}$$

where

$$\mathbf{A}(\mathbf{x}) = \sum_{a=1}^{n} w^a(\mathbf{x})\mathbf{p}(\mathbf{x}^a)\mathbf{p}^{\mathrm{T}}(\mathbf{x}^a),$$

$$\mathbf{B}(\mathbf{x}) = \left[w^1(\mathbf{x})\mathbf{p}(\mathbf{x}^1),\ w^2(\mathbf{x})\mathbf{p}(\mathbf{x}^2), \ldots, w^n(\mathbf{x})\mathbf{p}(\mathbf{x}^n)\right]. \tag{15}$$

The MLS approximation is well defined only when the matrix $\mathbf{A}$ in Eq. (14) is nonsingular. A necessary condition to satisfy this requirement is that at least m weight functions are non-zero (i.e. $n \geqslant m$) for each sample point $\mathbf{x} \in \Omega$ and that the nodes in Ω_x are not arranged in a special pattern such as on a straight line.

The solution of Eq. (14) for $\mathbf{a}(\mathbf{x}, s)$ and a subsequent substitution into Eq. (11) lead to the following relation

$$\bar{\theta}^h(\mathbf{x}, s) = \Phi^{\mathrm{T}}(\mathbf{x}) \cdot \hat{\theta}(s) = \sum_{a=1}^{n} \phi^a(\mathbf{x})\hat{\theta}^a(s), \tag{16}$$

where

$$\Phi^{\mathrm{T}}(\mathbf{x}) = \mathbf{p}^{\mathrm{T}}(\mathbf{x})\mathbf{A}^{-1}(\mathbf{x})\mathbf{B}(\mathbf{x}). \tag{17}$$

In Eq. (17), $\phi^a(\mathbf{x})$ is usually referred to as the shape function of the MLS approximation corresponding to the nodal point $\mathbf{x}^a$. From Eqs. (15) and (17), it can be seen that $\phi^a(\mathbf{x}) = 0$ when $w^a(\mathbf{x}) = 0$. In practical applications, $w^a(\mathbf{x})$ is often chosen such that it is non-zero over the support of the nodal point $\mathbf{x}^a$. The support of the nodal point $\mathbf{x}^a$ is usually taken to be a circle of the radius r^a centred at $\mathbf{x}^a$ (see Fig. 1). The radius r^a is an important parameter of the MLS approximation because it determines the range of the interaction (coupling) between the degrees of freedom defined at considered nodes.

A fourth-order spline-type weight function is applied in the present work

$$w^a(\mathbf{x}) = \begin{cases} 1 - 6\left(\frac{d^a}{r^a}\right)^2 + 8\left(\frac{d^a}{r^a}\right)^3 - 3\left(\frac{d^a}{r^a}\right)^4 & 0 \leqslant d^a \leqslant r^a \\ 0 & d^a \geqslant r^a, \end{cases} \tag{18}$$

where $d^a = \|\mathbf{x} - \mathbf{x}^a\|$ and r^a is the radius of the circular support domain. With Eq. (18), the C^1-continuity of the weight function is ensured over the entire domain, therefore the continuity condition of the heat flux is satisfied. The size of thesupport r^a should be large enough to cover a sufficient number of nodes in the domain of definition to ensure the regularity of the matrix $\mathbf{A}$. The value of n is determined by number of nodes lying in the support domain with radius r^a.

The partial derivatives of the MLS shape functions are obtained as [2]

$$\phi^a_{,k} = \sum_{j=1}^{m} \left[p^j_{,k}(\mathbf{A}^{-1}\mathbf{B})^{ja} + p^j(\mathbf{A}^{-1}\mathbf{B}_{,k} + \mathbf{A}^{-1}_{,k}\mathbf{B})^{ja} \right], \tag{19}$$

wherein $\mathbf{A}^{-1}_{,k} = \left(\mathbf{A}^{-1}\right)_{,k}$ represents the derivative of the inverse of $\mathbf{A}$ with respect to x_k, which is given by

$$\mathbf{A}^{-1}_{,k} = -\mathbf{A}^{-1}\mathbf{A}_{,k}\mathbf{A}^{-1}.$$

The directional derivatives of $\bar{\theta}(\mathbf{x}, s)$ are approximated in terms of the same nodal values as

$$\frac{\partial \bar{\theta}^h}{\partial n}(\mathbf{x}, s) = n_k(\mathbf{x}) \sum_{a=1}^{n} \hat{\theta}^a(s)\phi^a_{,k}(\mathbf{x}). \tag{20}$$

Then, the Laplace transform of the heat flux is approximated by

$$\bar{q}(\mathbf{x}, s) = k_{ij}(\mathbf{x})n_i(\mathbf{x}) \sum_{a=1}^{n} \hat{\theta}^a(s)\phi^a_{,j}(\mathbf{x}). \tag{21}$$

The local boundary integral equation (7) for the source point $\mathbf{x}^i$ located inside Ω yields the following set of equations:

$$\begin{aligned} &\sum_{a=1}^{n} \hat{\theta}^a(s) \int_{\partial\Omega_s^i} k_{ij}(\mathbf{x})n_i(\mathbf{x})\phi^a_{,j}(\mathbf{x})\mathrm{d}\Gamma \\ &- \sum_{a=1}^{n} \hat{\theta}^a(s) \int_{\Omega_s^i} \rho(\mathbf{x})c(\mathbf{x})s\phi^a(\mathbf{x})\mathrm{d}\Omega \\ &+ \sum_{a=1}^{n} \hat{\theta}^a(s) \int_{\Omega_s^i} \left[\frac{k_{rz}(\mathbf{x})}{r}\phi^a_{,z}(\mathbf{x}) + \frac{k_{rr}(\mathbf{x})}{r}\phi^a_{,r}(\mathbf{x}) \right]\mathrm{d}\Omega \\ &= -\int_{\Omega_s^i} \bar{F}(\mathbf{x}, s)\mathrm{d}\Omega. \end{aligned} \tag{22a}$$

For the source point $\mathbf{x}^i$ located on the global boundary Γ the boundary of the subdomain $\partial\Omega_s^i$ is created by L_s^i and Γ_{sq}^i(part of the global boundary with prescribed heat flux) according to Fig. 1. The local integral equation has in this case the following form:

$$\sum_{a=1}^{n}\hat{\theta}^a(s)\int\limits_{L_s^i}k_{ij}(\mathbf{x})n_i(\mathbf{x})\phi^a_{,j}(\mathbf{x})\mathrm{d}\Gamma$$
$$-\sum_{a=1}^{n}\hat{\theta}^a(s)\int\limits_{\Omega_s^i}\rho(\mathbf{x})c(\mathbf{x})s\phi^a(\mathbf{x})\mathrm{d}\Omega$$
$$+\sum_{a=1}^{n}\hat{\theta}^a(s)\int\limits_{\Omega_s^i}\left[\frac{k_{rz}(\mathbf{x})}{r}\phi^a_{,z}(\mathbf{x})+\frac{k_{rr}(\mathbf{x})}{r}\phi^a_{,r}(\mathbf{x})\right]\mathrm{d}\Omega$$
$$=-\int\limits_{\Gamma_{sq}^i}\tilde{\bar{q}}(\mathbf{x},s)\mathrm{d}\Gamma-\int\limits_{\Omega_s^i}\bar{F}(\mathbf{x},s)\mathrm{d}\Omega. \tag{22b}$$

It should be noted that there are neither Lagrange multipliers nor penalty parameters introduced into the local weak form (4) because the essential boundary conditions on $\Gamma^i_{s\theta}$ can be imposed directly using the interpolation approximation (16):

$$\sum_{a=1}^{n}\phi^a(\mathbf{x})\hat{\theta}^a(s)=\tilde{\bar{\theta}}(\mathbf{x}^i,s)\text{ for }\mathbf{x}^i\in\Gamma^i_{s\theta}, \tag{23}$$

where $\tilde{\bar{\theta}}(\mathbf{x}^i,s)$ is the Laplace transform of temperature prescribed on the boundary $\Gamma^i_{s\theta}$ for boundary conditions introduced below Eq. (2).

Similarly one can obtain the equation for unknown $\hat{\theta}^a(s)$ at nodes from the global boundary where natural conditions are prescribed. Set of algebraic equations (22) and (23) is used for computation of the Laplace transform of fictitious parameters $\hat{\theta}^a(s)$.

The time-dependent values of the transformed quantities in the previous consideration can be obtained by an inverse transform. There are many inversion methods available for the inverse Laplace transform. As the inverse Laplace transform is an ill-posed problem, small truncation errors can be greatly magnified in the inversion process and hence lead to poor numerical results. In the present analysis, the sophisticated Stehfest's algorithm [28] for the numerical inversion is used. If $\bar{f}(s)$ is the Laplace transform of $f(t)$, an approximate value f_a of $f(t)$ for a specific time t is given by

$$f_a(t)=\frac{\ln 2}{t}\sum_{i=1}^{N}v_i\,\bar{f}\left(\frac{\ln 2}{t}i\right), \tag{24}$$

where

$$v_i=(-1)^{N/2+i}$$
$$\sum_{k=[(i+1)/2]}^{\min(i,\,N/2)}\frac{k^{N/2}(2k)!}{(N/2-k)!\,k!\,(k-1)!\,(i-k)!\,(2k-i)!}. \tag{25}$$

Sutradhar et al. [30] have suggested to use $N=10$ for single precision arithmetic. It means that for each time t it is needed to solve N boundary value problems for the corresponding Laplace parameters $s=i\ln 2/t$, with $i=1,\,2,\,\ldots,\,N$. If M denotes the number of the time instants in which we are interested to know $f(t)$, the number of the Laplace transform solutions $\bar{f}(s_j)$ is then $M\times N$.

It is noteworthy that most of the alternative methods for the numerical inversion of the Laplace transform [9] require the use of complex valued Laplace transform parameter, and as a result, the application of complex arithmetic may lead to additional storage requirement and an increase in computing time.

4 Numerical examples

4.1 Full cylinder

An infinitely long full cylinder with a radius $a=1$ m loaded on its surface by a thermal shock with the Heaviside time step variation $\theta(a,t)=T\,H(t-0)$ where $T=1$ deg is considered firstly. Homogeneous material properties are assumed in the numerical analysis to check the accuracy of the proposed method. The diffusivity coefficient is chosen as $\kappa=1\,\mathrm{m^2s^{-1}}$. Since the boundary conditions along the cylinder are uniform we can consider a finite part of the cylinder in the numerical analysis with prescribed vanishing heat fluxes on both artificial cross sections of the cylinder. The cylinder can be created by the rotation of the rectangular plate ($a\times L$), where $2L$ is the length of the finite cylinder. Here, $L=1$ m is chosen. The temperature field on the finite square region is approximated by using 105 (5×21) nodes distributed in 5 layers in axial direction with 21 nodes equidistantly distributed in radial direction. Domains Ω_x are chosen identical to support domains Ω_x^i with $r^i=0.2$ m. Numerical results are compared with the analytical solution [7]:

$$\theta(r,t)=T-\frac{2T}{a}\sum_{n=1}^{\infty}T\frac{J_0(r\alpha_n)}{\alpha_n J_1(a\alpha_n)}\exp(-\kappa\alpha_n^2t), \tag{26}$$

where α_n are the roots of the following transcendental equation

$$J_0(a\alpha_n)=0$$

and J_0 and J_1 are first-type Bessel functions of zeroth and first order.

Both the Laplace transform and time-difference techniques were applied to solve the problem. For the Stehfest's numerical inversion of the Laplace transforms we have used ten different Laplace transform parameters. The time step was selected for the whole time interval as $\Delta t=0.04$ s. The time variation of the temperature on the axis of the cylinder is presented in Fig. 3, where an excellent agreement between the numerical and analytical results is obtained for the Laplace transform approach. In time difference technique the relative error of numerical results of temperature approaching the stationary quantity is about 1%. One way to increase the accuracy of the numerical scheme is the use of the second order backward difference scheme for the time derivative of the temperature in the governing Equation (2) [8].

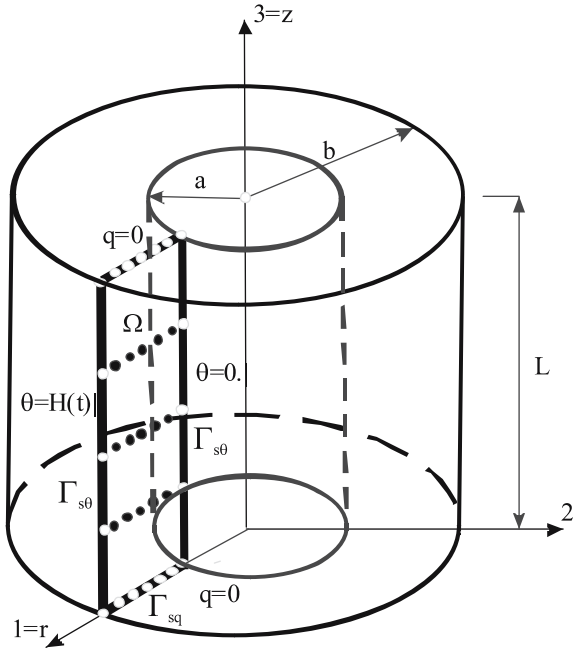

Fig. 2 Boundary conditions and node distribution in analysed domain for a finite hollow cylinder

4.2 Hollow cylinder

In the next example, we consider an infinitely long functionally graded thick-walled hollow cylinder with the radii $a = 4.0\,\text{m}$ and $b = 8.0\,\text{m}$ as depicted in Fig. 2. Since boundary conditions along the cylinder are considered to be uniform a finite part of the cylinder in the numerical analysis is selected with length $L = 4.0\,\text{m}$. On the external surface of the hollow cylinder the temperature, $\theta = 1\,\text{deg}$, is prescribed either stationarily or as Heaviside time-step thermal loading at time instant $t = 0$. The inner surface is kept at zero temperature. The mass density $\rho(\mathbf{x})$ and the specific heat

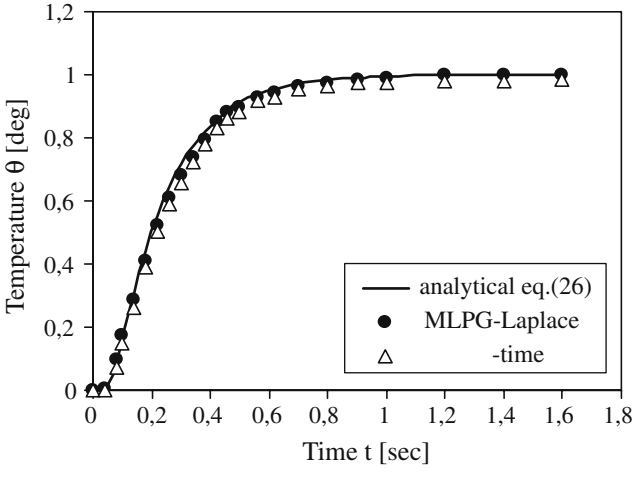

Fig. 3 Temporal evolution of temperature on the axis of a homogeneous full cylinder, subjected to Heaviside-type thermal loading at the jacket surface, at time instant $t = 0$

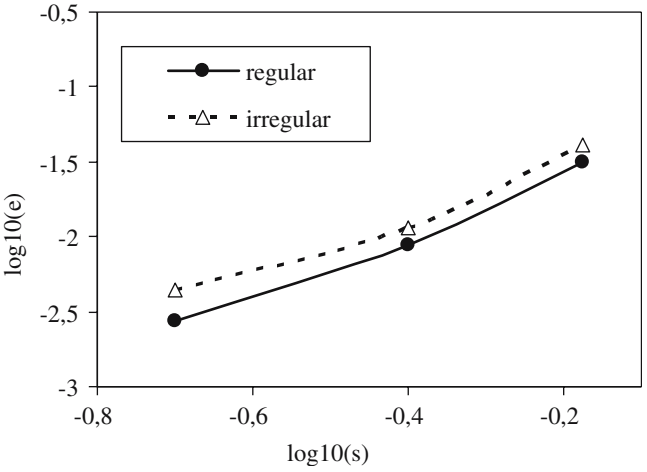

Fig. 4 Relative errors and convergence rates

$c(\mathbf{x})$ are considered to be uniform with $\rho = 1.0\,\text{kg/m}^3$ and $c = 1.0\,\text{Ws/kg deg}$. We consider a functionally graded hollow cylinder with the thermal conductivity being graded in the radial direction r as

$$k_{ij}(x) = k_{ij}^0 \exp\left[\gamma(r-a)\right]. \tag{27}$$

Isotropic material properties are considered in the first, $k_{ij}^0 = \delta_{ij}$ [W/m deg]. The exact solution for radial distribution of the stationary temperature in tube of exponentially graded material is given as [27]

$$\theta(r) = \theta(a) + \frac{\theta(b)-\theta(a)}{E_1(\gamma b) - E_1(\gamma a)}\left[E_1(\gamma r) - E_1(\gamma a)\right], \tag{28}$$

where $E_1(x)$ is the exponential integral function [1].

For this case an error and convergence analysis is studied. The relative percentage errors of L_2-norm are introduced for temperature as

$$e_\theta = \frac{\left\|\theta^{num} - \theta^{exact}\right\|}{\|\theta^{exact}\|},$$

where

$$\|\theta\| = \left(\int_\Omega (\theta)^2 d\Omega\right)^{1/2}.$$

The relative percentage errors and the convergence rates for three different node distributions are presented in Fig. 4, where s represents the node-distance on radial coordinate. The accuracy is very high (0,3%) especially for the finest node distribution consisting of 105 (21×5) nodes uniformly distributed in the rectangular domain with 21 nodes in the radial direction. In other two cases, 44 (11×4) and 24 (6×4) nodes have been used. The influence of the irregular node distribution on the accuracy is analysed too. At the vicinity of the corner, on internal radius ($r = a$) and $z = 0$, one additional node is included into the previous regular node

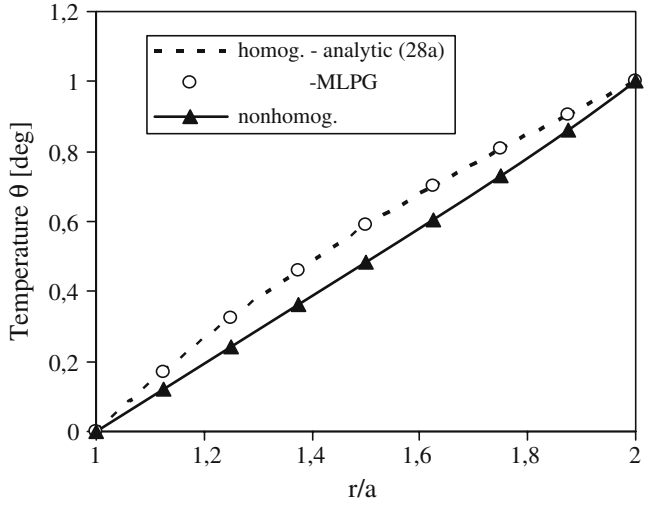

Fig. 5 Stationary radial temperature distribution in an isotropic FGM hollow cylinder with functional gradation parameter $\gamma = -0.2$

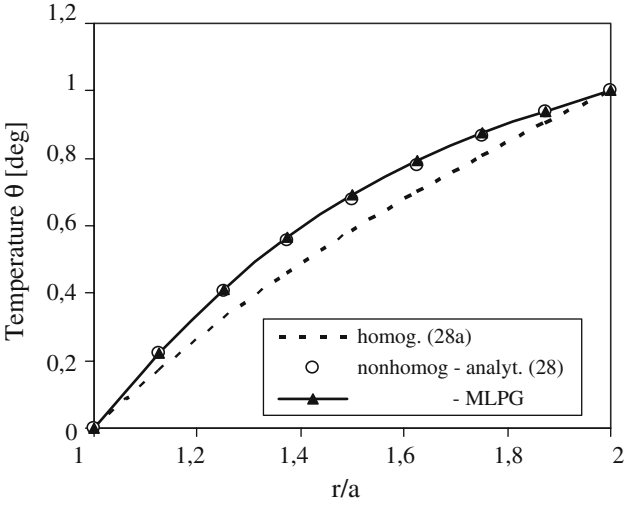

Fig. 6 Stationary radial temperature distribution in an isotropic FGM hollow cylinder with functional gradation parameter $\gamma = 0.2$ [see (27)]

distribution. Only one node is used to destroy the regularity of node distribution in all three densities. The coordinates of the additional node for the coarse-, middle- and finest-node distributions are (r=4,1; z=0,4), (4,2; 0,5) and (4,333; 0,5), respectively. One can observe on Fig. 4 very similar relative errors and convergence rates for both regular and irregular node distribution.

The radial variation of the temperature is an isotropic FGM hollow cylinder with $\gamma = -0.2$ under stationary temperature conditions is presented in Fig. 5 for temperature approximation with 150 nodes. In numerical analyses we have used the circular subdomain with radius $r_{toc} = 0.1m$ and support domain radius $r^i = 1m$.

Almost the same results were obtained for a twice larger support domain, however, computaional time grows with increasing support domain size. Numerical results were obtained by the Laplace transform technique. The dashed line is valid for a homogeneous hollow cylinder, where analytical solution is available too:

$$\theta(r) = \frac{\ln(r/a)}{\ln(b/a)}. \tag{28a}$$

One can observe a very good agreement of numerical and analytical results. The temperature for FGM cylinder with negative exponent of material gradation is lower than for the homogeneous cylinder within the whole radius since the thermal conductivity is also lower. Opposite situation is observed for the positive material gradation $\gamma = 0.2$. Results are presented on Fig. 6. One can observe a good agreement of results obtained by the MLPG and the analytical method given by Eq. (28) for an isotropic FGM hollow cylinder.

Next, a thermal shock on the external surface of the hollow cylinder is considered. For an isotropic homogeneous cylinder analytical solution is available [7]:

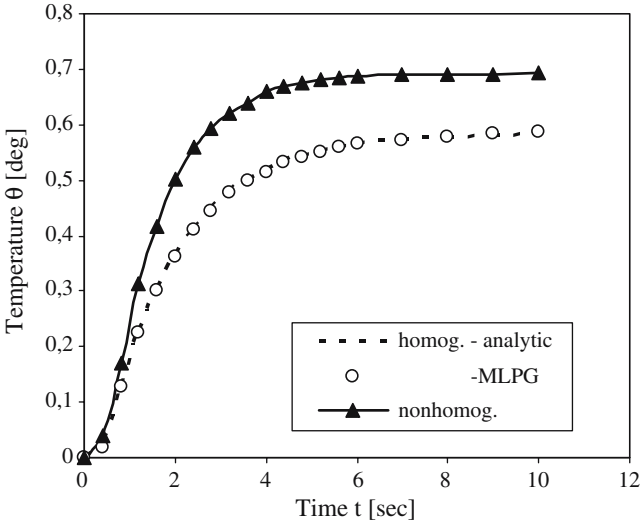

Fig. 7 Temporal evolution of the temperature in an isotropic FGM hollow cylinder with functional gradation parameter $\gamma = 0.2$ [see (27)], subjected to thermal shock on outer (jacket) surface, at time instant $t = 0$

$$\theta(r,t) = T\frac{\ln(r/R_1)}{\ln(R_2/R_1)} - \pi\sum_{n=1}^{\infty} T\frac{J_0^2(R_1\alpha_n)U_0(r\alpha_n)}{J_0^2(R_1\alpha_n) - J_0^2(R_2\alpha_n)}\exp(-\kappa\alpha_n^2 t), \tag{29}$$

where

$$U_0(r\alpha_n) = J_0(r\alpha_n)Y_0(\alpha_n R_2) - J_0(\alpha_n R_2)Y_0(r\alpha_n),$$

and α_n are the roots of the following transcendental equation

$$J_0(r)Y_0(rR_2/R_1) - J_0(rR_2/R_1)Y_0(r) = 0$$

with $J_0(r)$ and $Y_0(r)$ being the Bessel functions of the first and second kind and zeroth order.

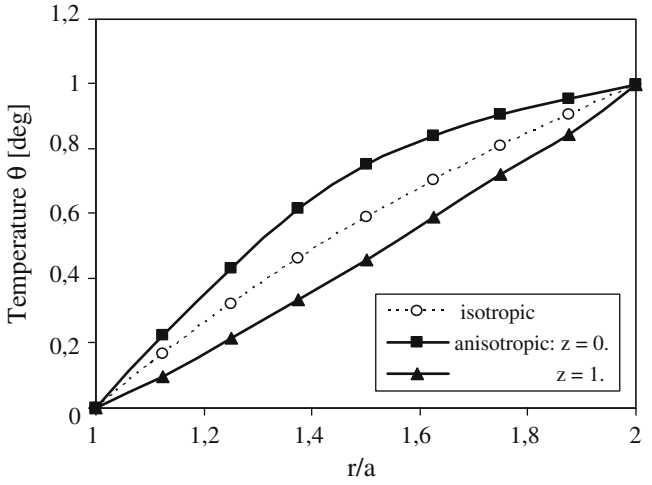

Fig. 8 Stationary radial temperature distribution in an anisotropic homogeneous hollow cylinder

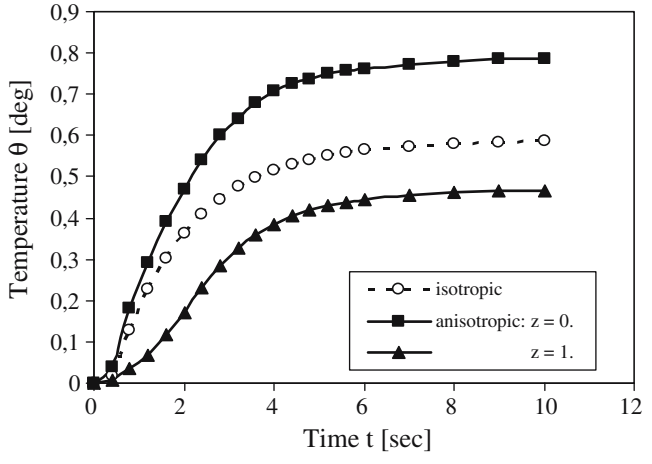

Fig. 9 Temporal evolution of the temperature at the mid radius in an anisotropic homogeneous hollow cylinder subjected to thermal shock on outer (jacket) surface, at time instant $t = 0$

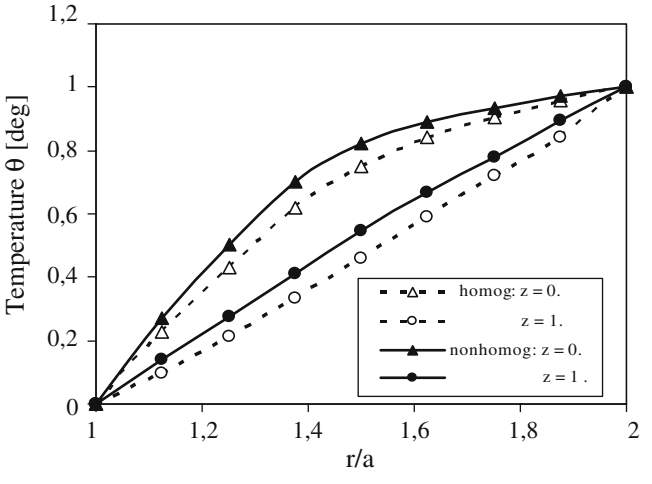

Fig. 10 Stationary radial temperature distribution in an anisotropic FGM hollow cylinder with functional gradation parameter $\gamma = 0.2$

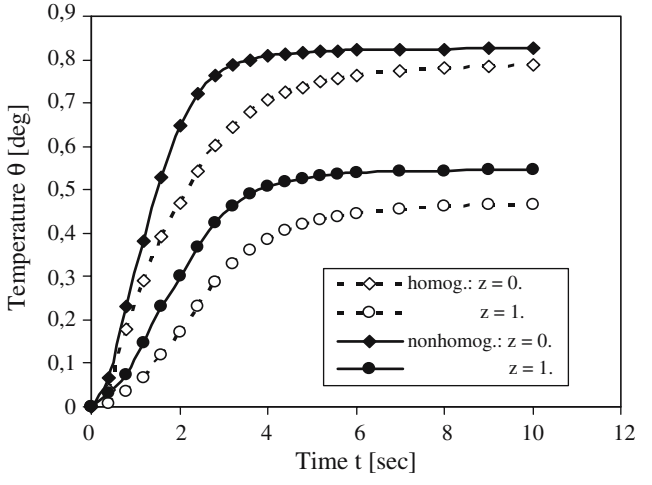

Fig. 11 Temporal evolution of the temperature at the mid radius in an anisotropic FGM hollow cylinder with functional gradation parameter $\gamma = 0.2$ [see (27)], subjected to thermal shock on outer (jacket) surface, at time instant $t = 0$

Numerical results for the mid radius, $r = 6.0$, presented by a dashed line in Fig. 7, are in a very good agreement with analytical ones. In the same figure the time variation of the temperature in isotropic FGM hollow cylinder with $\gamma = 0.2$ is given too.

Next, we consider a homogeneous anisotropic hollow cylinder with the same boundary conditions as in the isotropic case, and with thermal conductivity tensor of: $k_{rr} = 1$, $k_{zz} = 1.5$, $k_{rz} = 0.5$ W/m deg. Temperature variations with radial coordinate on upper and bottom sides are given in Fig. 8. The temperature variation with radial coordinate for the isotropic cylinder is lying between temperatures on bottom and upper sides of the anisotropic cylinder. The highest temperatures are observed on the bottom side of the cylinder. Time variations of the temperature at the mid radius and on the both ends of the cylinder under a thermal shock are given in Fig. 9. One can observe that temperatures are eventually approaching the stationary values.

Finally, we consider a functionally graded hollow cylinder with the thermal conductivity being graded in the radial direction r as described by Eq. (27), whereby $k^0_{rr} = 1$, $k^0_{zz} = 1.5$, $k^0_{rz} = 0.5$ W/m deg. Radial variations of the temperature in an anisotropic FGM hollow cylinder with $\gamma = 0.2$ under stationary temperature conditions are given in Fig. 10. The Heaviside time-step variation prescribed on the external surface of the cylinder is considered too. Time variations of the temperature at the mid radius in an anisotropic FGM hollow cylinder with $\gamma = 0.2$ under the thermal shock is given in Fig. 11.

It is interesting to investigate the influence of the material gradation on the temperature variation in the anisotropic hollow cylinder. Comparison of radial variations of the temperature in anisotropic FGM hollow cylinders for different material gradation under stationary and thermal shock conditions are presented in Figs. 12 and 13, respectively. A difference

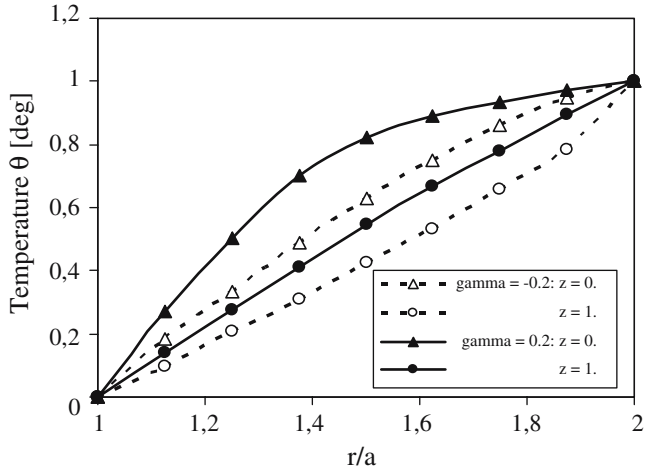

Fig. 12 Comparison of radial variations of the temperature in anisotropic FGM hollow cylinders for different material graduation under stationary temperature conditions

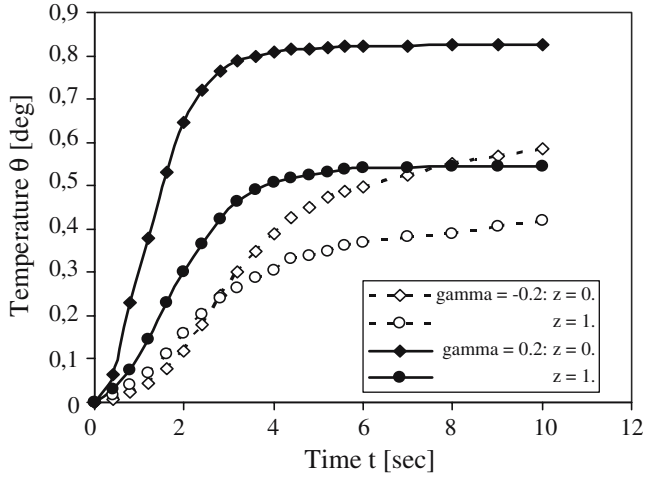

Fig. 13 Comparison of time variations of the temperature at the mid radius in anisotropic FGM hollow cylinders for different material graduation under thermal shock on outer surface

between temperatures on the bottom and upper sides of the cylinder is larger for material gradation $\gamma = 0.2$ than for the negative exponent $\gamma = -0.2$.

5 Conclusions

A local boundary integral equation method with the MLS approximation for spatial variations of physical fields together with using the Laplace transform technique for time variable is presented for transient heat conduction analysis in 3-D axisymmetric functionally graded bodies with continuously nonhomogeneous and anisotropic material properties. The initial-boundary value problem is solved in the Laplace transform domain with a subsequent numerical Laplace inversion to obtain time-dependent solutions. The boundary-domain formulation can be easily implemented on simple circular subdomains to which the local boundary integral equations are related. Contrary to the conventional boundary integral equation methods, all integrands in the present formulation are regular, thanks to the choice of a unit-step function as test function. Thus, no special integration techniques are required to evaluate the integrals. The present local boundary integral equation method removes the well-known restriction of the conventional BEM to problems with homogeneous material properties.

Acknowledgements The authors acknowledge the support by the Slovak Science and Technology Assistance Agency registered under number APVV-20-035404 and VEGA 2/6109/6. The cooperation between Bratislava and Vienna was made possible through a mobility grant from the Network of Excellence on Knowledge-based Multicomponent Materials (KMM-NoE) of the European Commission.

References

1. Abramowitz M, Stegun IA (1964) Handbook of mathematical functions. Applied mathematics series. Dover Publications, New York
2. Atluri SN (2004) The meshless method, (MLPG) for domain& BIE discretizations. Tech Science Press, Los Angeles, p 680
3. Atluri SN, Shen S (2002) The meshless local Petrov-Galerkin (MLPG) method. Tech Science Press, Los Angeles, p 440
4. Belytschko T, Krongauz Y, Organ D, Fleming M, Krysl P (1996) Meshless methods: an overview and recent developments. Comp Meth Appl Mech Eng 139:3–47
5. Brebbia CA, Telles JCF, Wrobel LC (1984) Boundary element techniques. Springer, Berlin, Heidelberg New York
6. Butterfield R (1978) An application of the boundary element method to potential flow problems in generally inhomogeneous bodies. In: Brebbia, CA (ed) Recent advances in boundary element method. Pentech Press, London
7. Carslaw HS, Jaeger JC (1959) Conduction of heat in solids. Clarendon Press, Oxford
8. Curran DA, Cross M, Lewis BA (1980) Solution of parabolic differential equations by the boundary element method using discretization in time. Appl Math Model 4:398–400
9. Davies B, Martin B (1979) Numerical inversion of the Laplace transform: a survey and comparison of methods. J Comput Phys 33:1–32
10. De S, Bathe KJ (2000) The method of finite spheres. Comput Mech 25:329–345
11. Erdogan F, Wu BH (1996) Crack problems in FGM layers under thermal stresses. J Therm Stresses 19:237–265
12. Jin ZH (2002) An asymptotic solution of temperature field in a strip of a functionally graded material. Int Commun Heat Mass 29:887–895
13. Jin ZH, Noda N (1993) An internal crack parallel to the boundary of a nonhomogeneous half plane under thermal loading. Int J Eng Sci 31:793–806
14. Jin ZH, Batra RC (1996) Stress intensity relaxation at the tip of an edge crack in a functionally graded material subjected to a thermal shock. J Therm Stresses 19:317–339
15. Jin ZH, Paulino GH (2001) Transient thermal stress analysis of an edge crack in a functionally graded material. Int J Fracture 107: 73–98
16. Kim JH, Paulino GH (2002) Isoparametric graded finite elements for nonhomogeneous isotropic and orthotropic materials. J Appl Mech 69:502–514
17. Lancaster P, Salkauskas K (1981) Surfaces generated by moving least square methods. Math Comput 37:141–158
18. Mikhailov SE (2002) Localized boundary-domain integral formulations for problems with variable coefficients. Eng Anal Boundary Elem 26:681–690

19. Miyamoto Y, Kaysser WA, Rabin BH, Kawasaki A, Ford RG (1999) Functionally Graded Materials; Design, Processing and Applications. Kluwer, Dordrecht
20. Nayroles B, Touzot G, Villon P (1992) Generalizing the finite element method. Comput Mech 10:307–318
21. Noda N, Jin ZH (1993) Thermal stress intensity factors for a crack in a strip of a functionally gradient material. Int J Solids Struct 30:1039–1056
22. Noda N, Jin ZH (1994) A crack in functionally gradient materials under thermal shock. Arch Appl Mech 64:99–110
23. Sladek J, Sladek V, Zhang Ch (2003a) Transient heat conduction analysis in functionally graded materials by the meshless local boundary integral equation method. Comput Mater Sci 28: 494–504
24. Sladek J, Sladek V, Krivacek J, Zhang Ch (2003b) Local BIEM for transient heat conduction analysis in 3-D axisymmetric functionally graded solids. Comput Mech 32:169–176
25. Sladek J, Sladek V, Atluri SN (2004a) Meshless local Petrov-Galerkin method for heat conduction problem in an anisotropic medium. CMES – Comput Model Eng Sci 6:309–318
26. Sladek J, Sladek V, Zhang Ch (2004b) A meshless local boundary integral equation method for heat conduction analysis in nonhomogeneous solids. J Chin Inst Eng 27:517–539
27. Sladek V, Sladek J, Zhang Ch (2005) Local integro-differential equations with domain elements for the numerical solution of partial differential equations with variable coefficients. J Eng Math 51:261–282
28. Stehfest H (1970) Algorithm 368: numerical inversion of Laplace transform. Commun Assoc Comput Mach 13:47–49
29. Suresh S, Mortensen A (1998) Fundamentals of functionally graded materials. Institute of Materials, London, p 165
30. Sutradhar A, Paulino GH, Gray LJ (2002) Transient heat conduction in homogeneous and non-homogeneous materials by the Laplace transform Galerkin boundary element method. Eng Anal Bound Elem 26:119–132
31. Tanaka M, Tanaka K (1980) Transient heat conduction problems in inhomogeneous media discretized by means of boundary-volume element. Nucl Eng Des 60:381–387
32. Zhu T, Zhang JD, Atluri SN (1998) A local boundary integral equation (LBIE) method in computational mechanics, and a meshless discretization approach. Comput Mech 21:223–235